frontiers in Energy Research

ORIGINAL RESEARCH
published: 24 March 2020
doi: 10.3389/fenrg.2020.00046

Functionally Decorated Carbon Nanotube Networks for Energy Storage in Supercapacitors

Mohamed Nawwar[1], *Rakesh P. Sahu*[1,2], *Ishwar K. Puri*[1,2] *and Igor Zhitomirsky*[1]*

[1] *Department of Materials Science and Engineering, McMaster University, Hamilton, ON, Canada,* [2] *Department of Mechanical Engineering, McMaster University, Hamilton, ON, Canada*

A novel approach has been developed for the fabrication of Fe_3O_4 decorated multiwalled carbon nanotubes (MWCNT) for energy storage in negative electrodes of electrochemical supercapacitors. Synthesis of Fe_3O_4 was performed in the presence of MWCNT, dispersed using various cationic and anionic polyaromatic dispersants. The comparison of experimental results obtained using different dispersants provided an insight into the influence of the chemical structure of the dispersant molecules on the microstructure of the Fe_3O_4-MWCNT materials. It was found that positively charged groups and chelating catechol ligands of the dispersants facilitated the formation of Fe_3O_4 decorated MWCNT with low agglomeration. The Fe_3O_4 -MWCNT materials, prepared using different dispersants were used for the fabrication of electrodes with mass loading of 40 mg cm^{-2}. The highest capacitance was obtained in 0.5 M Na_2SO_4 electrolyte for Fe_3O_4 decorated MWCNT prepared using cationic celestine blue dye as a dispersant. Improved cyclic voltammetry profile was obtained using FeOOH as an additive. Asymmetric devices were fabricated and tested based on the Fe_3O_4 decorated MWCNT negative electrodes and MnO_2-MWCNT positive electrodes.

Keywords: carbon nanotube, iron oxide, energy, supercapacitor, dispersant

OPEN ACCESS

Edited by:
Kaiyuan Shi,
National Research Council Canada, Canada

Reviewed by:
Zhenyu Xing,
South China Normal University, China
Dan Luo,
University of Waterloo, Canada

***Correspondence:**
Igor Zhitomirsky
zhitom@mcmaster.ca

Specialty section:
This article was submitted to Electrochemical Energy Conversion and Storage, a section of the journal Frontiers in Energy Research

Received: *19 February 2020*
Accepted: *05 March 2020*
Published: *24 March 2020*

Citation:
Nawwar M, Sahu RP, Puri IK and Zhitomirsky I (2020) Functionally Decorated Carbon Nanotube Networks for Energy Storage in Supercapacitors. Front. Energy Res. 8:46. doi: 10.3389/fenrg.2020.00046

INTRODUCTION

Electrochemical supercapacitors are currently under intensive investigation for energy storage and capacitive water purification applications (Shi et al., 2014; Zhao and Zheng, 2015; Ding et al., 2020). Research is focused on the development of new materials and electrolytes (Brousse and Bélanger, 2003; Shi and Zhitomirsky, 2010; Li et al., 2019), fabrication of nanoparticles of active materials (Luo et al., 2016; Silva et al., 2018), design and modeling of composite electrodes and devices (Pavaskar et al., 2018; Xing et al., 2019). New strategies have been designed for the fabrication of carbon based electrodes with enhanced capacitive performance (Salinas Torres et al., 2019). Significant interest has been generated in application of carbon nanotubes (CNT) for the fabrication of composite electrode materials (Lu et al., 2019). The interest in CNT applications for supercapacitors is related to high electronic conductivity and high surface area of CNT.

It was recognized that CNT can be decorated with other functional materials (Pan et al., 2015; Hao et al., 2016). With a desire to fabricate new and advanced devices, there is growing interest in the development of new techniques for the fabrication of functionally decorated CNT, such as laser ablation (Imbrogno et al., 2017), atomic layer deposition (Ding et al., 2018), polymerization

(Zhu et al., 2014), magnetron sputtering (Wei et al., 2014), electrodeposition (Chitturi et al., 2016), and chemical precipitation (Hong et al., 2013). Decorated CNT are of particular interest for energy storage and generation devices, such as supercapacitors, batteries, and fuel cells. The use of functionally decorated CNT allowed for the fabrication of advanced batteries with enhanced capacity (Hong et al., 2013; Wei et al., 2014), good cyclic stability (Chitturi et al., 2016) and improved conductivity (Wang et al., 2010). It has been reported that CNT can be decorated with catalysts for advanced application in fuel cells (Sonkar et al., 2017). Significant advances have been achieved in applications of functionally decorated CNT for photovoltaic devices (Mathew et al., 2011; Tai et al., 2014). It has previously been shown that carbon nanotubes can be decorated with oxides (Ojha et al., 2019), polypyrrole (Su and Zhitomirsky, 2015) and activated carbon (Shi et al., 2014) for energy storage applications in supercapacitors.

Previous studies highlighted the need in the development of efficient manufacturing techniques for the fabrication of functionally decorated CNT. Such techniques need to be based on the careful selection of dispersing agents, which must be well adsorbed on the CNT surface. Good dispersion of CNT is critical for their decoration with functional materials. The use of networks of decorated CNT is promising for the fabrication of advanced supercapacitor electrodes with high active mass.

The objective of this investigation was the fabrication of Fe_3O_4 decorated CNT for application in negative electrodes of asymmetric supercapacitors. Following this objective we investigated anionic and cationic aromatic dispersants for the dispersion of CNT. The results presented below indicated that chemical precipitation of Fe_3O_4 in the presence of CNT allowed for the fabrication of Fe_3O_4 decorated CNT. Testing results provided an insight into the influence of electric charge and chelating groups of the dispersants on the Fe_3O_4 formation on the CNT surface. The fibrous networks of decorated CNT were used for the fabrication of negative electrodes with high active mass of 40 mg cm^{-2}. The capacitive behavior was linked to dispersant structure. Finally, we fabricated and tested an asymmetric supercapacitor device.

EXPERIMENTAL PROCEDURES

Iron (II) chloride tetrahydrate ($FeCl_2{\cdot}4H_2O$), iron (III) chloride hexahydrate ($FeCl_3{\cdot}6H_2O$), ammonium hydroxide (NH_4OH), sodium hydroxide (NaOH), sodium sulfate (Na_2SO_4), palmetic acid (PA), celestine blue (CB), pyrocatechol violet (PV), azure A chloride (AA), m-cresol purple (CP), poly (vinyl butyral-co-vinyl-alcohol-co-vinyl-acetate) (PVB, average MW = 50,000-80,000), multiwalled carbon nanotubes (MWCNT, purity > 95 %, OD 20-30 nm, and length 1–2 μm, US Nanomaterial Inc, USA), and Ni foam (porosity of 95%, Vale Ltd., Canada) were used.

For decoration of the MWCNT by Fe_3O_4 nanoparticles, the synthesis of the nanoparticles was performed in the presence of dispersed MWCNT. In this procedure, 1 g L^{-1} of MWCNT were dispersed in DI water by ultrasonication for 15 min and then 0.25 g L^{-1} dispersant was added and suspension was ultrasonicated again for 15 min. A stoichiometric mixture of Fe^{2+} and Fe^{3+} salts dissolved in DI water was added to the suspension of MWCNT in order to obtain the mass ratio of Fe_3O_4 to MWCNT equal to 1.5. The pH was adjusted to 9 by the addition of 1 M NH_4OH. The obtained suspension was ultrasonicated for 40 min and then filtrated. The materials were washed with DI water and dried overnight. The magnetite decorated MWCNT, prepared using CB, PV, AA, and CP were denoted as M-CB-MWCNT, M-PV-MWCNT, M-AA-MWCNT, and M-CP-MWCNT, respectively. Non-agglomerated FeOOH nanoparticles were prepared by a chemical precipitation and liquid-liquid extraction method (Chen et al., 2019). However, in contrast to the previous investigation (Chen et al., 2019) PA was used as a new and efficient extractor. M-FH-CB-MWCNT material was prepared by mixing of M-CB-MWCNT (80%) and FeOOH (20%).

M-CB-MWCNT, M-PV-MWCNT, M-AA-MWCNT, M-CP-MWCNT, and M-FH-CB-MWCNT were dispersed in ethanol, containing dissolved PVB binder and obtained slurries were used for the impregnation of Ni foam current collectors and fabrication of negative electrodes of supercapacitors. The PVB binder content in the electrodes was 3%. The total mass of the impregnated material was 40 mg cm^{-2}. MnO_2-MWCNT material for positive electrodes was prepared by the precipitation and liquid-liquid extraction method (Chen et al., 2017). The asymmetric device was fabricated containing M-FH-CB-MWCNT negative electrodes with mass loading of 40 mg cm^{-2} and MnO_2-MWCNT positive electrodes with mass loading of 35 mg cm^{-2}. At such mass loadings the capacitance of negative electrodes matched the capacitance of the positive electrodes.

Transmission electron microscopy was performed (dark field STEM) using a JEOL 2010F field emission microscope. X-ray diffraction (XRD) analysis was performed using the Bruker D8 Discover instrument comprising Davinci diffractometer and Co-Kα radiation. Particle size distribution was done using dynamic light scattering (DLS) model (DelsaMax Pro- Beckman Coulter). The analysis was carried out based on testing of 4 sets of each material with a concentration of 0.4 mg L^{-1} in DI, where every set consisted of 10 acquisition.

Cyclic voltammetry (CV) and electrochemical impedance spectroscopy (EIS) studies of single electrodes and asymmetric device were performed in 0.5 L of 0.5 M Na_2SO_4 electrolyte as described in prior investigations (Shi and Zhitomirsky, 2013; Zhu et al., 2014; Chen et al., 2017). EIS measurements were carried out in the frequency range of 10 mHz−100 kHz with a sinusoidal signal of 10 mV. The components of complex capacitance (C′s and C″s) were calculated from the EIS data as $C's = Z''/\omega|Z|^2A$ and $C''s = Z'/\omega|Z|^2A$, where $\omega = 2\pi f$ and f is frequency. Galvanostatic charge–discharge of individual electrodes at different current densities was performed using Biologic VMP 300 potentiostat. The charge-discharge behavior of the asymmetric device was analyzed using battery analyzers BST8-MA and BST8-3 (MTI Corporation, USA).

RESULTS AND DISCUSSION

Figures 1A–D shows chemical structures of aromatic dispersants used for dispersion of MWCNT. The polyaromatic structure of the dispersants was beneficial (Ata et al., 2018) for their adsorption on MWCNT. The adsorption mechanism involved π-π interactions. The adsorbed dispersants imparted a positive charge (CB, AA) or a negative charge (PV, CP) to MWCNT. The small size, electric charge and good adsorption of the dispersants on MWCNT facilitated MWCNT dispersion by unzipping mechanism (Ata et al., 2018; **Figure 1E**) and allowed for the fabrication of stable suspensions. **Figures 1F,G** illustrates different types of interactions of the dispersants with Fe_3O_4 particles. The precipitation of Fe_3O_4 was achieved at pH = 9, which is above the isoelectric point (pH = 6.5) (Parks, 1965) of this material. Therefore, the Fe_3O_4 particles were negatively charged. The negative charge of Fe_3O_4 resulted in electrostatic repulsion of Fe_3O_4 and anionic PV or CP, adsorbed on MWCNT (**Figure 1F**). In contrast, electrostatic attraction existed between Fe_3O_4 and cationic CB or AA molecules, adsorbed on MWCNT (**Figure 1G**). Previous investigations (Ata et al., 2014) showed that molecules, containing a catechol group, strongly adsorbed on inorganic particles, and facilitated their efficient dispersion. Therefore, CB and PV can be adsorbed on Fe_3O_4 particles by catecholate type bonding. **Figure 1F** shows bonding of PV to the Fe atom on the particle surface. A similar mechanism can be suggested for CB bonding. It is important to note that phenolic molecules containing single OH groups, such as CP, show poor adsorption on inorganic molecules (Ata et al., 2014). In contrast, molecules from the catechol family, such as PV, containing two adjacent OH groups, show very strong bonding to the inorganic particles (Ata et al., 2014).

X-ray diffraction studies confirmed the formation of pure Fe_3O_4 by precipitation from mixed Fe^{2+} and Fe^{3+} salt solutions (**Figure S1**). The materials prepared by precipitation from the same solutions, containing dispersed MWCNT, showed X-ray diffraction peaks of Fe_3O_4 and MWCNT (**Figure 2**). Peak broadening resulted from the small particle size of Fe_3O_4. TEM analysis revealed influence of the dispersants on the material morphologies. **Figure 3** shows TEM images of the materials at different magnifications. The TEM images of M-CB-MWCNT showed the formation of Fe_3O_4 decorated MWCNT. The size of the Fe_3O_4 particles adsorbed on the MWCNT was about 10 nm. It is suggested that electrostatic attraction of positively charged CB dispersant and negatively charged Fe_3O_4 as well as chelating bonding of the catechol group facilitated the formation of the decorated MWCNT. It is important to note that electrostatic repulsion of the PV dispersant, adsorbed on the MWCNT surface, and Fe_3O_4 nanoparticles was detrimental for the formation of the decorated MWCNT. On the other hand, the chelating bonding of the catechol groups of PV promoted Fe_3O_4 formation on the MWCNT surface. The chelating bonding was a dominating mechanism, which allowed for the formation of decorated MWCNT. However, the TEM studies of M-PV-MWCNT also revealed the formation of small agglomerates of the Fe_3O_4 particles as it is shown in **Figure 3F**. The analysis of the TEM images for M-AA-MWCNT and M-CP-MWCNT showed enhanced agglomeration of the Fe_3O_4 particles. The agglomeration is especially evident for M-CP-MWCNT samples. In this case the

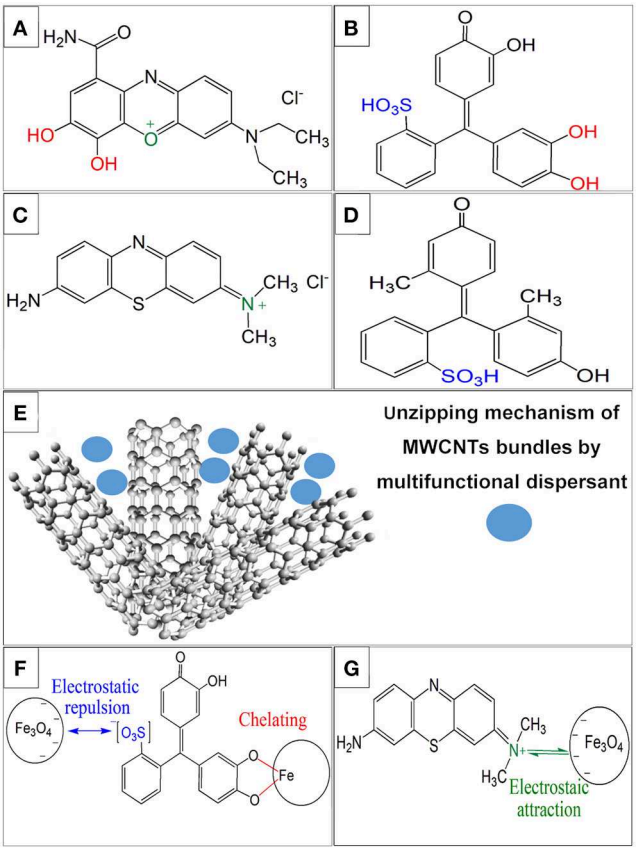

FIGURE 1 | Chemical structures of **(A)** CB, **(B)** PV, **(C)** AA, **(D)** CP and schematics, showing **(E)** unzipping of MWCNT bundles by dispersants, **(F)** electrostatic repulsion of PV and Fe_3O_4 particles and chelating bonding of PV to Fe atoms on the Fe_3O_4 particle surface, involving a catechol group of PV, **(G)** electrostatic attraction of AA and Fe_3O_4.

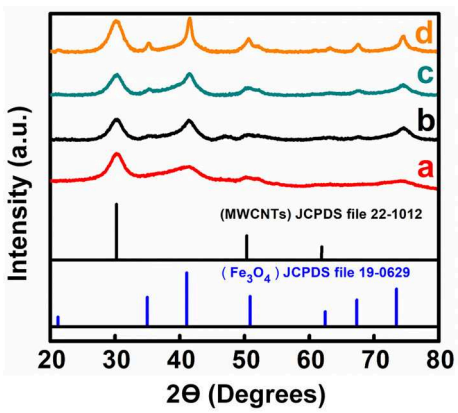

FIGURE 2 | X-ray diffraction patterns of (a) M-CB-MWCNT, (b) M-PV-MWCNT, (c) M-AA-MWCNT, and (d) M-CP-MWCNT.

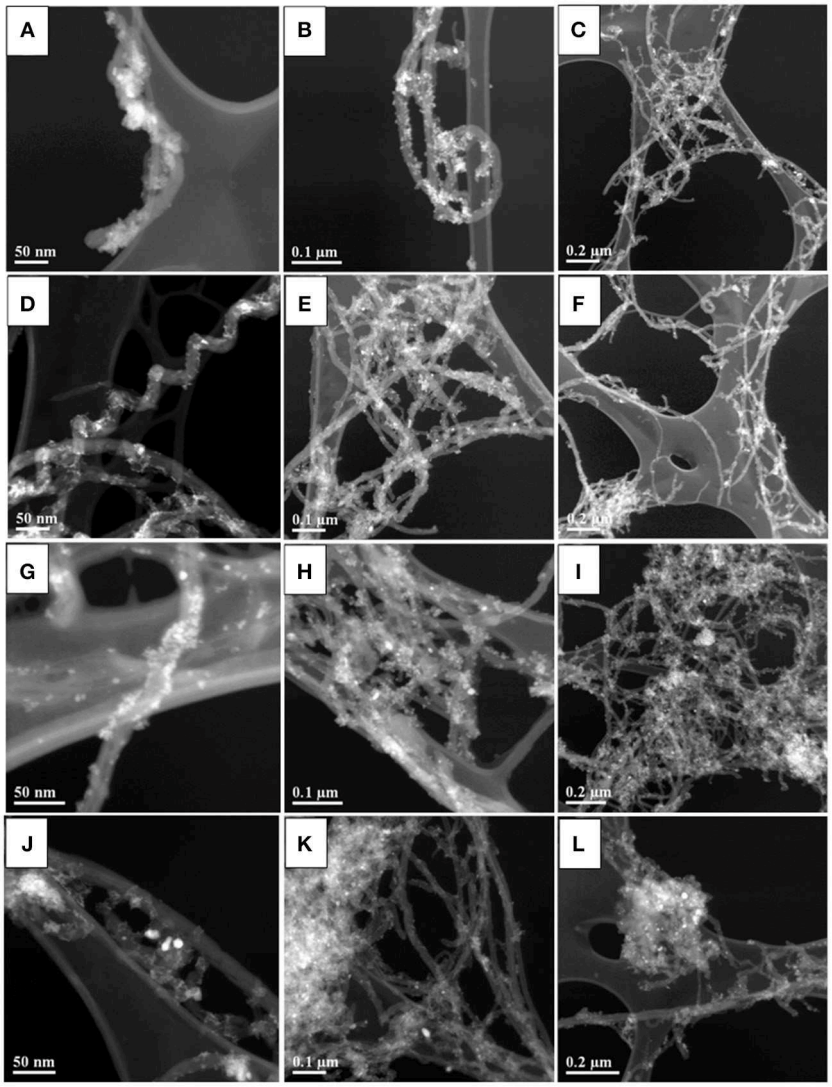

FIGURE 3 | TEM images at different magnifications for **(A–C)** M-CB-MWCNT, **(D–F)** M-PV-MWCNT, **(G–I)** M-AA-MWCNT, and **(J–L)** M-CP-MWCNT.

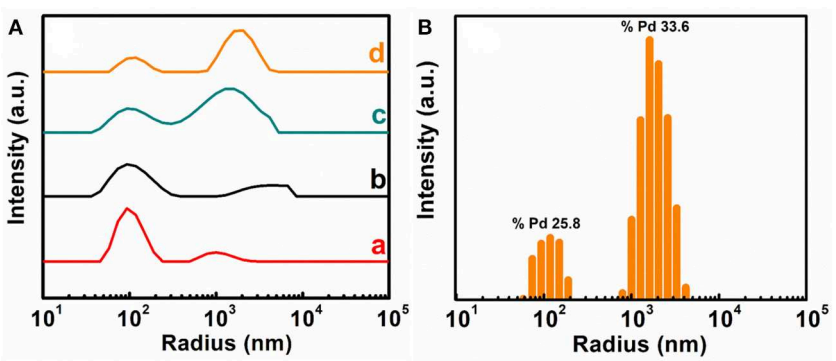

FIGURE 4 | (A) Average data (40 samples of each composition) for DLS analysis of (a) M-CB-MWCNT, (b) M-PV-MWCNT, (c) M-AA-MWCNT and (d) M-CP-MWCNT, **(B)** Typical spectrum for M-CP-MWCNT. The width of the peaks indicates the polydispersity of the aggregate (Pd).

poor coverage of MWCNT resulted from electrostatic repulsion of CP and Fe_3O_4.

The effect of different dispersing agents has also been studied using DLS analysis (**Figure 4**). The size distribution of the aggregates in all samples is bimodal with different degree of polydispersity. The first peak at ∼100 nm is present in all four dispersions with different intensities. The second peak was observed in the range of 10^3-10^4 nm. The intensity and polydispersity of the second peak are smallest for M-CB-MWCNT. The polydispersity of M-PV-MWCNT is broader than that of M-CB-MWCNT. The analysis of the DLS data for M-AA-MWCNT and M-CP-MWCNT revealed significant increase in the relative intensity of the second peak, compared to the intensity of the first peak. The second peak for M-AA-MWCNT and M-CP-MWCNT shifted to larger radius numbers, compared to the second peak for M-CB-MWCNT. The increase in relative intensity of the second peak for M-AA-MWCNT and M-CP-MWCNT and peak shifts indicated an increasing number of agglomerates and increase in the agglomerate size of the particles. This is in agreement with the TEM data and indicates the beneficial effect of the catechol groups of CB and PV for the formation of decorated MWCNT and reduction of Fe_3O_4 agglomeration. It is important to note that the decoration of MWCNT resulted from the dispersant mediated adsorption. In this approach the changes in MWCNT structure, resulting from chemical reactions and high temperature treatment (Xing et al., 2015, 2017, 2019) can be avoided.

M-CB-MWCNT, M-PV-MWCNT, M-AA-MWCNT, M-CP-MWCNT were used for the fabrication of supercapacitor electrodes with mass loading of 40 mg cm^{-2}. **Figure 5** shows cyclic voltammetry data for the electrodes in the potential range of −0.9 to 0.0 V vs. SCE. M-CB-MWCNT electrodes showed a larger CV area, compared to other electrodes and higher integral capacitance in the selected potential window. The M-CP-MWCNT electrodes showed lower capacitance, compared to

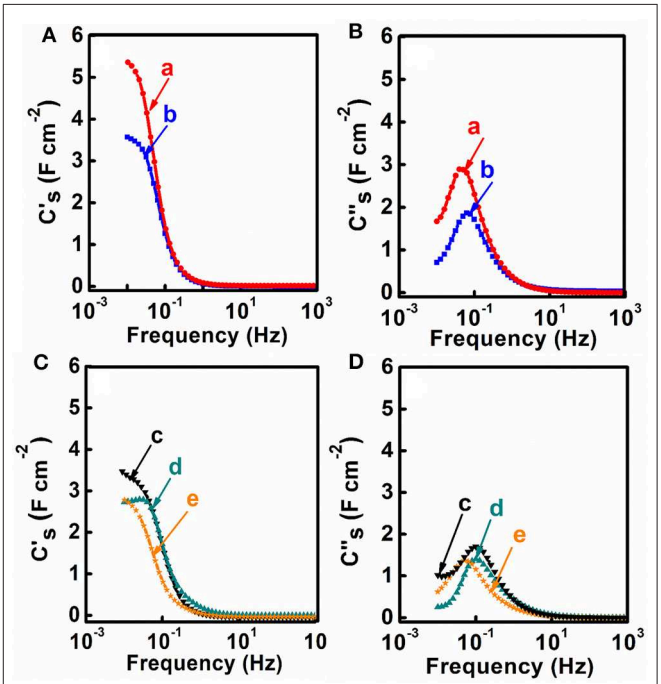

FIGURE 6 | (A–D) Frequency dependences of components of complex AC capacitance, calculated from impedance data for (a) M-CB-MWCNT, (b) M-FH-CB-MWCNT, (c) M-PV-MWCNT, (d) M-AA-MWCNT and (e) M-CP-MWCNT electrodes.

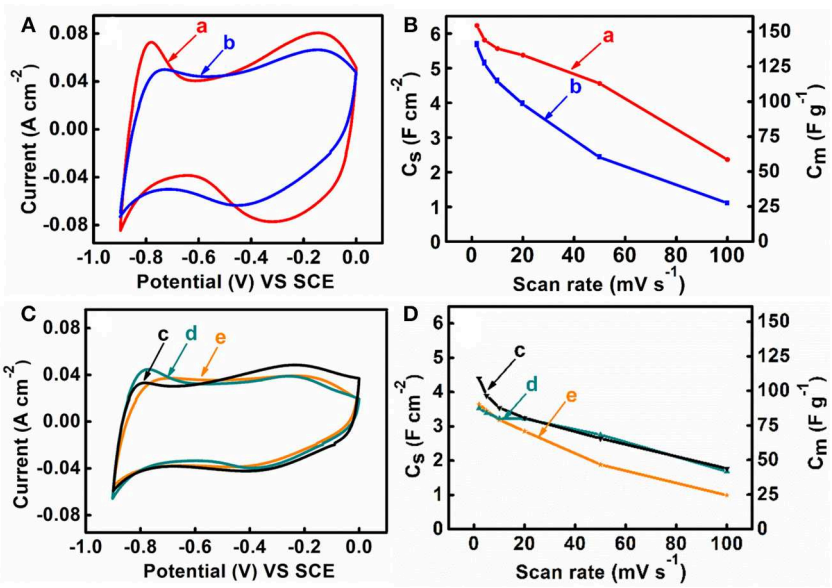

FIGURE 5 | (A,C) CVs and **(B,D)** capacitance vs. scan rate for (a) M-CB-MWCNT, (b) M-FH-CB-MWCNT, (c) M-PV-MWCNT, (d) M-AA-MWCNT and (e) M-CP-MWCNT electrodes.

other materials. The higher capacitance of M-CB-MWCNT can result from reduced agglomeration of the Fe_3O_4 particles and improved contact of Fe_3O_4 and MWCNT. However, the CV for M-CB-MWCNT showed redox peaks and deviated significantly from the box shape. Significant reduction of the charge and discharge currents was observed in the potential range of −0.4 to −0.7 V. The observed redox peak can result from the redox-active properties of CB (Noorbakhsh et al., 2008). Such CV shape is detrimental for the fabrication of asymmetric cells. In order to improve the CV profile, the M-CB-MWCNT was combined with FeOOH, which shows good charge storage properties in the range of −0.4 to −0.7 V (Chen et al., 2018). Therefore, M-FH-CB-MWCNT was prepared and tested. This material showed improved CV shape, compared to M-CB-MWCNT. The capacitance of 5.76 F cm^{-2} (144 F g^{-1}) was obtained at a scan rate of 2 mV s^{-1}. **Figure 6** shows frequency dependences of the components of differential AC capacitance, calculated from the impedance data. M-CB-MWCNT showed the highest real part of capacitance C'_S at low frequencies, compared to other materials. However, the M-FH-CB-MWCNT electrodes showed lower C''_S, which indicated lower energy losses. The slightly higher relaxation frequency, corresponding to maximum of C''_S, indicated better performance. The M-CP-MWCNT electrodes, showed lower C'_S and lower relaxation frequency, compared to other materials. The capacitive behavior of the electrodes has also been analyzed by chronopotentiometry. **Figure 7** compares galvanostatic charge-discharge curves for different electrodes and capacitances, calculated from the discharge data at different current densities. The charge-discharge curves were of nearly triangular shape. The highest capacitance at 3 mA

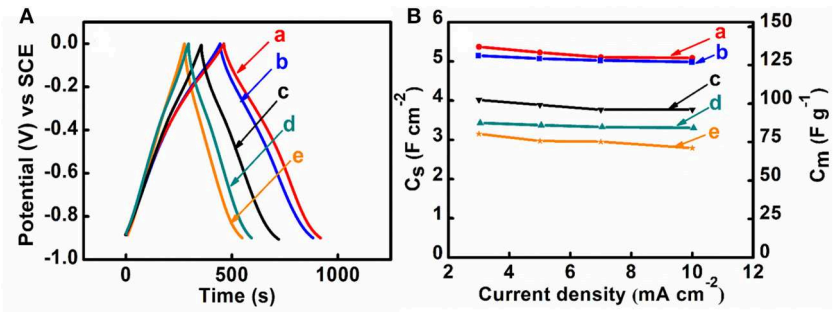

FIGURE 7 | (A) Charge-discharge curves at current density of 5 mA cm^{-2}, **(B)** capacitance, calculated from charge-discharge data, vs. current density for (a) M-CB-MWCNT, (b) M-FH-CB-MWCNT, (c) M-PV-MWCNT, (d) M-AA-MWCNT and (e) M-CP-MWCNT.

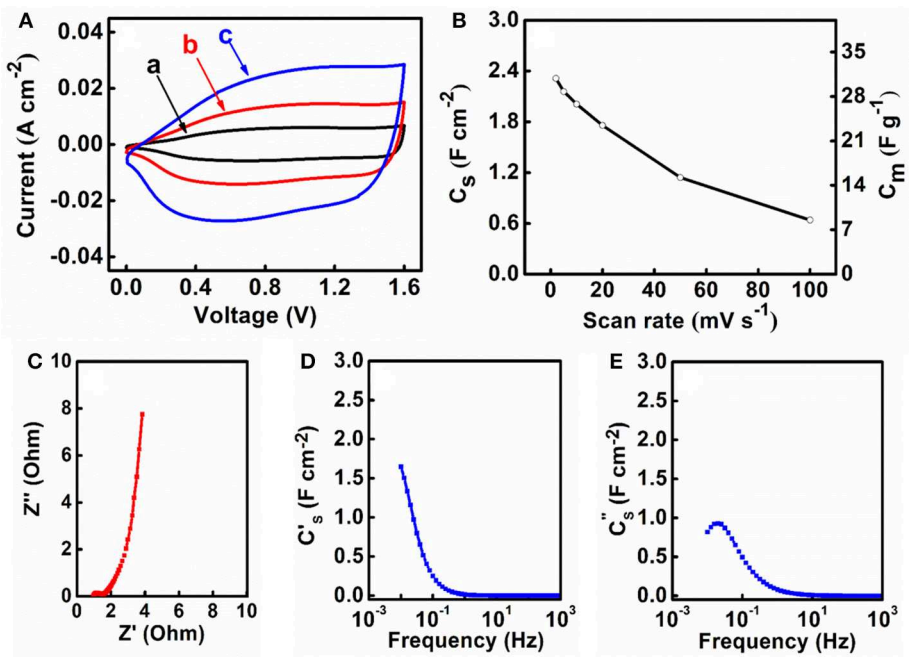

FIGURE 8 | (A) CVs at scan rates of (a) 2, (b) 5 and (c) 10 mV s^{-1}, **(B)** C_S and C_m calculated from the CV data vs. scan rate, **(C)** Nyquist plot of complex impedance and frequency dependences of **(D)** C'_s and **(E)** C''_s for an asymmetric supercapacitor cell, containing M-FH-CB-MWCNT as a negative electrode and MnO_2-MWCNT as a positive electrode.

cm^{-2} was achieved using M-CP-MWCNT. However, M-FH-CB-MWCNT showed benefits of nearly constant capacitance in the range of 3–10 mA cm^{-2}. The M-CP-MWCNT and M-FH-CB-MWCNT electrodes showed practically the same capacitances at 5 and 10 mA cm^{-2}. The M-CP-MWCNT electrodes showed significantly lower capacitance, compared to other electrodes in agreement with CV and impedance spectroscopy data.

M-FH-CB-MWCNT electrodes were used for the fabrication of the asymmetric supercapacitor cells. One of the problems related to the fabrication of asymmetric devices with Na_2SO_4 electrolyte is related to lower capacitance of negative electrodes, compared to the capacitance of advanced positive electrodes, such as MnO_2-MWCNT (Chen et al., 2017). However, M-FH-CB-MWCNT electrodes showed relatively high capacitance and the asymmetric device was fabricated using 40 mg cm^{-2} M-FH-CB-MWCNT negative electrode and 35 mg cm^{-2} MnO_2-MWCNT positive electrode. It is known that aqueous asymmetric devices based on Fe_3O_4 negative electrodes and MnO_2 positive electrodes (Brousse and Bélanger, 2003) can operate in a voltage window of 1.8. Water decomposition can be avoided due to overpotential for oxygen evolution. **Figure 8A** shows CVs for the device in a voltage window of 1.6 V. The current increased with increasing scan rate. As expected, the capacitance C_S of the device was about 50% of the capacitance of the individual electrodes (**Figure 8B**). The device showed relatively low impedance and relatively high relaxation frequency (**Figures 8C–E**). The asymmetric devices showed ideal triangular shape charge-discharge curves (**Figure 9A**, inset). The capacitance slightly decreased (**Figure 9A**) with current density in the range of 3-50 mA cm^{-2}. The capacitance retention after 1,000 cycles was 75% (**Figure 9B**). The Coulombic efficiency remained about 100% during cycling. The device had an energy density of about 1 mWh cm^{-2} which showed relatively small variations with increasing current density in the range of 3–50 mA cm^{-2} (**Figure 9C**). Two cells, connected in series, allowed for the powering of eleven 20 mA LEDs, as it is shown in **Figure 9D**.

CONCLUSIONS

Polyaromatic CB, PV, AA, and CP molecules allowed for efficient dispersion of MWCNT. The chelating catechol groups of CB and PV as well as electrostatic attraction of cationic CB and AA with negatively charged Fe_3O_4 particles were beneficial for the formation of Fe_3O_4 decorated MWCNT. M-CB-MWCNT showed a network of Fe_3O_4 decorated MWCNT and low agglomeration of Fe_3O_4 nanoparticles. M-CB-MWCNT exhibited higher capacitance, compared to M-PV-MWCNT, M-AA-MWCNT and M-CP-MWCNT. Compared to M-CB-MWCNT, the M-FH-CB-MWCNT electrodes showed improved CV profile, reduced AC energy losses and low variation of capacitance with increasing charge-discharge current.

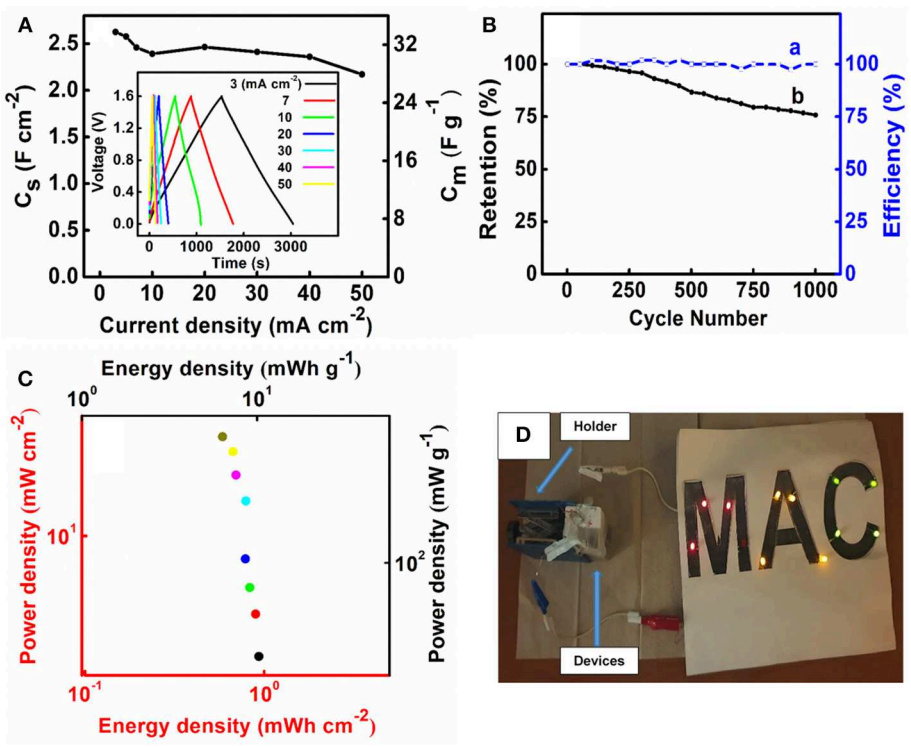

FIGURE 9 | (A) C_S and C_m vs. current density calculated from discharge data, inset shows charge-discharge curves, and different current densities, **(B)** (a) Coulombic efficiency and (b) capacitance retention and vs. cycle number, **(C)** Ragone plot for an asymmetric supercapacitor cell, containing M-FH-CB-MWCNT as a negative electrode and MnO_2-MWCNT as a positive electrode, **(D)** LEDs powered by two asymmetric cells.

M-FH-CB-MWCNT showed good capacitive behavior at mass loading of 40 mg cm^{-2}. Asymmetric devices were fabricated, containing M-FH-CB-MWCNT negative electrodes and MnO_2-MWCNT positive electrodes, which showed promising capacitance and power-energy characteristics.

DATA AVAILABILITY STATEMENT

The datasets generated for this study are available on request to the corresponding author.

AUTHOR CONTRIBUTIONS

MN conducted synthesis of materials, performed materials characterization and electrochemical testing, analysis of the data and contributed to the writing of the manuscript. RS contributed to DLS and electron microscopy testing, data analysis, and writing of the manuscript. IZ contributed to the development of new dispersants, cell design. IP and IZ contributed to the data analysis and writing of the manuscript.

FUNDING

This work was supported by the Natural Sciences and Engineering Research Council of Canada.

ACKNOWLEDGMENTS

The authors would like to thank the Natural Sciences and Engineering Research Council of Canada for the financial support. Dr. Carmen Andrei of Canadian Centre for Electron Microscopy (CCEM), M.A.Sc. Victoria Jarvis of McMaster Analytical X-Ray Diffraction Facility for XRD for assistance with measurements, and Dr. R. Poon for fruitful discussions and technical support.

SUPPLEMENTARY MATERIAL

The Supplementary Material for this article can be found online at: https://www.frontiersin.org/articles/10.3389/fenrg.2020.00046/full#supplementary-material

REFERENCES

Ata, M., Liu, Y., and Zhitomirsky, I. (2014). A review of new methods of surface chemical modification, dispersion and electrophoretic deposition of metal oxide particles. *RSC Adv.* 4, 22716–22732. doi: 10.1039/c4ra02218a

Ata, M. S., Poon, R., Syed, A. M., Milne, J., and Zhitomirsky, I. (2018). New developments in non-covalent surface modification, dispersion and electrophoretic deposition of carbon nanotubes. *Carbon* 130, 584–598. doi: 10.1016/j.carbon.2018.01.066

Brousse, T., and Bélanger, D. (2003). A hybrid fe3o4-mno2 capacitor in mild aqueous electrolyte. *Electrochem Solid-State Lett.* 6, A244–A248. doi: 10.1149/1.1614451

Chen, R., Poon, R., Sahu, R. P., Puri, I. K., and Zhitomirsky, I. (2017). Mno2-carbon nanotube electrodes for supercapacitors with high active mass loadings. *J. Electrochem. Soc.* 164, A1673–A1678. doi: 10.1149/2.1491707jes

Chen, R., Puri, I., and Zhitomirsky, I. (2019). Polypyrrole-carbon nanotube-feooh composites for negative electrodes of asymmetric supercapacitors. *J. Electrochem. Soc.* 166, A935–A940. doi: 10.1149/2.0281906jes

Chen, R., Puri, I. K., and Zhitomirsky, I. (2018). High areal capacitance of feooh-carbon nanotube negative electrodes for asymmetric supercapacitors. *Ceram. Int.* 44, 18007–18015. doi: 10.1016/j.ceramint.2018.07.002

Chitturi, V. R., Ara, M., Fawaz, W., Ng, K. Y. S., and Arava, L. M. R. (2016). Enhanced lithium–oxygen battery performances with pt subnanocluster decorated n-doped single-walled carbon nanotube cathodes. *ACS Catal.* 6, 7088–7097. doi: 10.1021/acscatal.6b01016

Ding, H., Zhang, Q., Liu, Z., Wang, J., Ma, R., Fan, L., et al. (2018). Tio2 quantum dots decorated multi-walled carbon nanotubes as the multifunctional separator for highly stable lithium sulfur batteries. *Electrochim. Acta* 284, 314–320. doi: 10.1016/j.electacta.2018.07.167

Ding, Y., Wang, T., Dong, D., and Zhang, Y. (2020). Using biochar and coal as the electrode material for supercapacitor applications. *Front. Energy Res.* 7:159. doi: 10.3389/fenrg.2019.00159

Hao, M., Tang, M., Wang, W., Tian, M., Zhang, L., and Lu, Y. (2016). Silver-nanoparticle-decorated multiwalled carbon nanotubes prepared by poly (dopamine) functionalization and ultraviolet irradiation. *Compos. B. Eng.* 95, 395–403. doi: 10.1016/j.compositesb.2016.03.084

Hong, H. P., Kim, M. S., Lee, Y. H., Yu, J. S., Lee, C. J., and Min, N. K. (2013). Spray deposition of limn2o4 nanoparticle-decorated multiwalled carbon nanotube films as cathode material for lithium-ion batteries. *Thin Solid Films* 547, 68–71. doi: 10.1016/j.tsf.2013.05.002

Imbrogno, A., Pandiyan, R., Barberio, M., Macario, A., Bonanno, A., and El khakani, M. A. (2017). Pulsed-laser-ablation based nanodecoration of multi-wall-carbon nanotubes by co-ni nanoparticles for dye-sensitized solar cell counter electrode applications. *Mater. Renewable Sustainable Energy* 6:11. doi: 10.1007/s40243-017-0095-3

Li, X., Huang, Z., and Zhi, C. (2019). Environmental stability of mxenes as energy storage materials. *Front. Mater.* 6:312. doi: 10.3389/fmats.2019.00312

Lu, Z., Raad, R., Safaei, F., Xi, J., Liu, Z., and Foroughi, J. (2019). Carbon nanotube based fiber supercapacitor as wearable energy storage. *Front. Mater.* 6:138. doi: 10.3389/fmats.2019.00138

Luo, D., Wallar, C. J., Shi, K., and Zhitomirsky, I. (2016). Enhanced capacitive performance of mno2-multiwalled carbon nanotube electrodes, prepared using lauryl gallate dispersant. *Colloids Surfaces A* 509, 504–511. doi: 10.1016/j.colsurfa.2016.09.065

Mathew, A., Rao, G. M., and Munichandraiah, N. (2011). Dye sensitized solar cell based on platinum decorated multiwall carbon nanotubes as catalytic layer on the counter electrode. *Mater. Res. Bull.* 46, 2045–2049. doi: 10.1016/j.materresbull.2011.07.001

Noorbakhsh, A., Salimi, A., and Sharifi, E. (2008). Fabrication of glucose biosensor based on encapsulation of glucose-oxidase on sol-gel composite at the surface of glassy carbon electrode modified with carbon nanotubes and celestine blue. *Electroanalysis* 20, 1788–1797. doi: 10.1002/elan.200804245

Ojha, M., Le Houx, J., Mukkabla, R., Kramer, D., Andrew Wills, R. G., and Deepa, M. (2019). Lithium titanate/pyrenecarboxylic acid decorated carbon nanotubes hybrid - alginate gel supercapacitor. *Electrochim. Acta* 309, 253–263. doi: 10.1016/j.electacta.2019.03.211

Pan, Y., Hu, W., Liu, D., Liu, Y., and Liu, C. (2015). Carbon nanotubes decorated with nickel phosphide nanoparticles as efficient nanohybrid electrocatalysts for the hydrogen evolution reaction. *J. Mater. Chem. A* 3, 13087–13094. doi: 10.1039/C5TA02128F

Parks, G. A. (1965). The isoelectric points of solid oxides, solid hydroxides, and aqueous hydroxo complex systems. *Chem. Rev.* 65, 177–198. doi: 10.1021/cr60234a002

Pavaskar, G., Ramakrishnasubramanian, K., Kandagal, V. S., and Kumar, P. (2018). Modeling electric double-layer capacitors using charge variation methodology in gibbs ensemble. *Front. Energy Res.* 5:36. doi: 10.3389/fenrg.2017.00036

Salinas Torres, D., Ruiz-Rosas, R., Morallon, E., and Cazorla-Amorós, D. (2019). Strategies to enhance the performance of electrochemical capacitors based on carbon materials. *Front. Mater.* 6:115. doi: 10.3389/fmats.2019.00115

Shi, C., and Zhitomirsky, I. (2010). Electrodeposition and capacitive behavior of films for electrodes of electrochemical supercapacitors. *Nanoscale Res. Lett.* 5:518. doi: 10.1007/s11671-009-9519-z

Shi, K., Ren, M., and Zhitomirsky, I. (2014). Activated carbon-coated carbon nanotubes for energy storage in supercapacitors and capacitive water purification. *ACS Sustain. Chem. Eng.* 2, 1289–1298. doi: 10.1021/sc500118r

Shi, K., and Zhitomirsky, I. (2013). Electrophoretic nanotechnology of graphene–carbon nanotube and graphene–polypyrrole nanofiber composites for electrochemical supercapacitors. *J. Colloid Interface Sci.* 407, 474–481. doi: 10.1016/j.jcis.2013.06.058

Silva, R. M. E., Poon, R., Milne, J., Syed, A., and Zhitomirsky, I. (2018). New developments in liquid-liquid extraction, surface modification and agglomerate-free processing of inorganic particles. *Adv. Colloid Interface Sci.* 261, 15–27. doi: 10.1016/j.cis.2018.09.005

Sonkar, P. K., Prakash, K., Yadav, M., Ganesan, V., Sankar, M., Gupta, R., et al. (2017). Co(ii)-porphyrin-decorated carbon nanotubes as catalysts for oxygen reduction reactions: An approach for fuel cell improvement. *J. Mater. Chem. A* 5, 6263–6276. doi: 10.1039/C6TA10482G

Su, Y., and Zhitomirsky, I. (2015). Asymmetric electrochemical supercapacitor, based on polypyrrole coated carbon nanotube electrodes. *Appl. Energy* 153, 48–55. doi: 10.1016/j.apenergy.2014.12.010

Tai, S.-Y., Lu, M.-N., Ho, H.-P., Xiao, Y., and Lin, J.-Y. (2014). Investigation of carbon nanotubes decorated with cobalt sulfides of different phases as nanocomposite catalysts in dye-sensitized solar cells. *Electrochim. Acta* 143, 216–221. doi: 10.1016/j.electacta.2014.07.145

Wang, T., Kaempgen, M., Nopphawan, P., Wee, G., Mhaisalkar, S., and Srinivasan, M. (2010). Silver nanoparticle-decorated carbon nanotubes as bifunctional gas-diffusion electrodes for zinc-air batteries. *J. Power Sources* 195, 4350–4355. doi: 10.1016/j.jpowsour.2009.12.137

Wei, W., Ruiz, I., Ahmed, K., Bay, H. H., George, A. S., Wang, J., et al. (2014). Silicon decorated cone shaped carbon nanotube clusters for lithium ion battery anodes. *Small* 10, 3389–3396. doi: 10.1002/smll.201400088

Xing, Z., Deng, Y.-P., Sy, S., Tan, G., Li, A., Li, J., et al. (2019). Carbon-pore-sheathed cobalt nanoseeds: an exceptional and durable bifunctional catalyst for zinc-air batteries. *Nano Energy* 65, 104051. doi: 10.1016/j.nanoen.2019.104051

Xing, Z., Qi, Y., Tian, Z., Xu, J., Yuan, Y., Bommier, C., et al. (2017). Identify the removable substructure in carbon activation. *Chem. Mater.* 29, 7288–7295. doi: 10.1021/acs.chemmater.7b01937

Xing, Z., Wang, B., Halsted, J. K., Subashchandrabose, R., Stickle, W. F., and Ji, X. (2015). Direct fabrication of nanoporous graphene from graphene oxide by adding a gasification agent to a magnesiothermic reaction. *Chem. Commun.* 51, 1969–1971. doi: 10.1039/C4CC08977D

Zhao, C., and Zheng, W. (2015). A review for aqueous electrochemical supercapacitors. *Front. Energy Res.* 3:23. doi: 10.3389/fenrg.2015.00023

Zhu, Y., Shi, K., and Zhitomirsky, I. (2014). Polypyrrole coated carbon nanotubes for supercapacitor devices with enhanced electrochemical performance. *J. Power Sources* 268, 233–239. doi: 10.1016/j.jpowsour.2014.06.046

Conflict of Interest: The authors declare that the research was conducted in the absence of any commercial or financial relationships that could be construed as a potential conflict of interest.

The handling editor declared a past co-authorship with one of the authors IZ.